A phase-field model for interphase precipitation in V-micro-alloyed structural steels

Alireza Rahnama*, Samuel Clark, Vit Janik, Seetharaman Sridhar

Advanced Steel Research Centre, University of Warwick, CV4 7AL, United Kingdom

Abstract

A multi-component phase field model was developed based on CALPHAD method and directly coupled with the CALPHAD thermodynamic database using a four-sublattice model. Interphase carbide precipitation at the γ/α interface is simulated and the predictions are tested against reported experimental results for a medium carbon, vanadium micro-alloyed steel during an isothermal $\gamma \rightarrow \alpha + MC$ transformation at 973 K. The model is found to be able to accurately predict: interphase precipitate composition, morphology and size of the precipitates. Furthermore, the *tip-to-tip* pairing of interphase precipitates in γ/α interphase boundaries is elucidated and found to be attributable to the minimisation of interfacial energy.

Keywords: Phase-field, CALPHAD, Interphase Precipitation, Hight Strength Steel.
2010 MSC: 00-01, 99-00

1. Introduction

The development of new hot-rolled high-strength, whilst formable steels, offer great potential for novel lightweight automotive chassis components [1]. In particular, hot-rolled High Strength Steels (HSS) with both high strength and excellent stretch-flange formability are particularly promising [2] for automotive component down-gauging and the forming of innovative geometries. Steels with a single ferritic matrix

*Corresponding author
Email addresses: A.Rahnama@warwick.ac.uk (Alireza Rahnama), S.J.Clark@warwick.ac.uk (Samuel Clark), V.Janik@warwick.ac.uk (Vit Janik), S.Seetharaman@warwick.ac.uk (Seetharaman Sridhar)

phase strengthened with a fine distribution of interphase carbide precipitates offer opportunities for a low cost alternative that can be more easily processed in the liquid state and continuously cast compared to higher alloyed advanced high strength steels.[3]. Interphase precipitation consists of periodic rows of carbide precipitates which form simultaneously at the interphase boundary between the decomposing austenite and growing ferrite [4]. Desired mechanical properties are achieved by controlling the spacing between the rows and spacing between the particles within a row. The augmentation of alloying and thermo-mechanical processing in order to achieve the necessary combination of mechanical properties however, presents a significant challenge requiring principally, the optimisation of precipitation in hot-rolled AHSS. The purpose of this work is to provide a developmental step in the understanding of precipitation phenomena and elucidating the nature of precipitation at interphase interfaces in multi-component alloys.

1.1. Interphase Precipitation

Interphase precipitation is observed in an array of steel alloys containing strong carbonitride forming elements and such as; V, Nb, Ti, Mo, Cr, W [5]. Precipitates are formed in planar regular sheets as shown in Figure 1. Typically, carbonitride second phase particles, which have been formed through the interphase precipitation phenomena are highly uniform both in terms of size and orientation [6]. The precipitates formed are typically rich in carbon as it is significantly enriched at the γ/α interphase boundary [7] whereas, the the enrichment of nitrogen appears to be very limited [8], as such for modelling purposes they shall be considered to be purely carbides in this work. The precipitates are conventionally thought to invariably obey a single variant the Baker-Nutting orientation relationship, BN OR [9]. Although, the generality of this finding has been questioned [10]. In cases where the ferrite and the austenite into which it grows are related by the Kurdjumov-Sachs relationship, KS OR, $(111)_\gamma \parallel (110)_\alpha$, the particular variant will be that which makes the close packed planes of all three phases (γ, α, and precipitate) parallel. This minimises the free energy required for nuclei formation [7]. An alternate explanation is that the variant selection is determined

by the influence of the angular relationship between the facet upon a precipitate embryo penetrating beyond both sides of the γ/α interphase boundary and the resulting free energy of activation for nucleation [11].

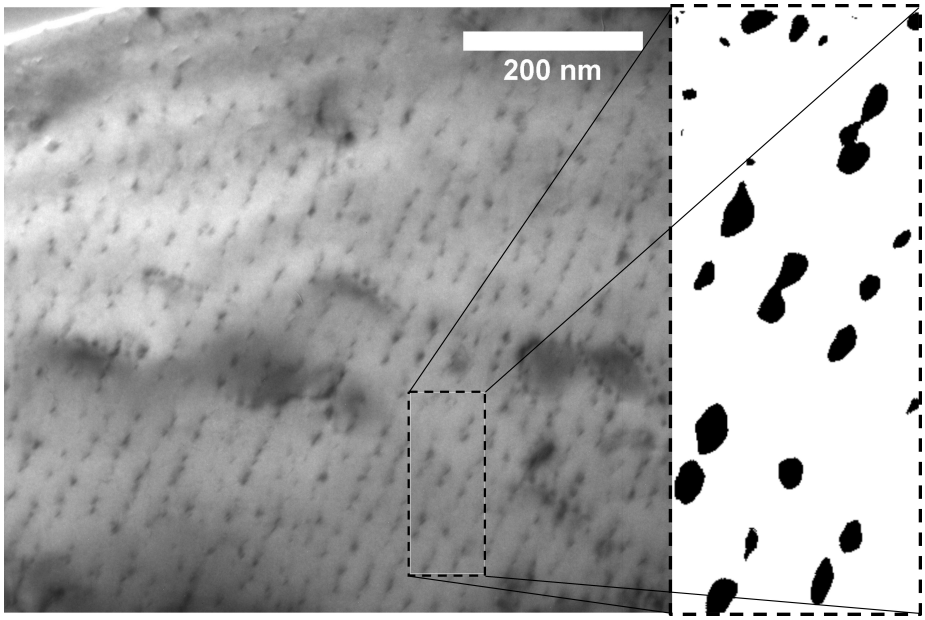

Figure 1: Typical planar rows of interphase precipitates in an Fe-1.62Mn-0.19V-0.2Mo-0.19Si-0.045C $wt\%$ alloy isothermally transformed at 973 K for 5 $mins$ and a digitally processed binary image section showing precipitate twinning.

1.2. Modelling of Interphase Precipitation

In order to develop alloys and processes capable of exploiting the full potential of the interphase precipitation detailed microstructural models must be developed. A number of analytical models have been previously developed [12, 13, 14, 15, 16, 17, 18, 19, 20], which have primarily focussed upon the prediction of spacing between sheets of interphase carbides. Although, this enables some guidance of the the processing windows for hot-rolled automotive sheets a more holistic modelling approach with the capability to simultaneously predict the morphology and nature of interphase carbide precipitates [21] as well as the inter-sheet spacing is required to truly optimise processing. To fill this gap in the knowledge, and in order to capture the nature of the

interphase precipitation a fundamentally different modelling approach was required, a phase field model (PFM), which has yet to have been applied to the interphase precipitation reaction was considered. The scope of the model developed was to predict; interphase precipitate composition, morphology and size as a function of temperature and time.

The use, basic principles and potential of PFM's for exploring a wide range of microstructural evolution and related phenomena have been reviewed in detail by Chen [22] and Militzer [23]. A particular strength of the PFM approach is that complex models exploring morphologically complex features can be readily simulated [23] such as, the precipitation of κ-carbide in low density steels developed in our research group [24].

2. The Present Model

Due to the wealth of experimental data from several studies on a similar alloy [25, 26, 27, 28], including Small angle X-Ray and Neutron Scattering (SAX and SANS) [26] an abridged Fe-Mn-V-C quaternary composition using the values for the respective elements outlined in Table 1 has been adopted. Although the presented model is applicable to a system with many components, we considered a quaternary system of Fe-Mn-V-C because firstly we wanted to report the basics of our model and avoid complications and secondly there was no experimental data available in the literature reporting the interphase precipitation while all Ti, Mo,V, and other alloying elements are present in the system. A more complex model which also includes the elastic strain energy and binding energy terms has been also developed based on the presented model and will be reported in our future paper. The experimental knowledge of this is supplemented by the studies on the effect of γ/α OR upon interphase precipitation of Furuhara and co-workers [29, 30] and the 3D atom probe tomography, APT of Nöhrer [8] on lower C V-micro-alloyed steels.

Mukherjee *et al.* demonstrated by APT, studies that the partitioning behaviour of interphase precipitates greatly depends on the alloying elements [31, 32]. Here, a four sub-lattice model was employed in order to make the interchange between Fe and Mn atoms possible during the computation.

Table 1: Modelled composition from abridged from Refs. [26, 27] at% bal. Fe.

C	Mn	V
1.962	0.748	0.312

The order parameters and the concentrations for Mn, V, and C were expressed as:

$$\phi_i^1 = \frac{(y_i^{(1)} - y_i^{(2)} - y_i^{(3)} + y_i^{(4)})}{4c_i} \quad i = Mn, C, V \tag{1a}$$

$$\phi_i^2 = \frac{(y_i^{(1)} - y_i^{(2)} + y_i^{(3)} - y_i^{(4)})}{4c_i} \quad i = Mn, C, V \tag{1b}$$

$$\phi_i^3 = \frac{(y_i^{(1)} + y_i^{(2)} - y_i^{(3)} - y_i^{(4)})}{4c_i} \quad i = Mn, C, V \tag{1c}$$

$$c_i = \frac{(y_i^{(1)} + y_i^{(2)} + y_i^{(3)} + y_i^{(4)})}{4} \quad i = Mn, C, V \tag{1d}$$

In this way, each site fraction $y_i^{(s)}$ can be rewritten as function of order parameters ϕ_i^s. Although the choice of eq.1a-d make the model more complicated, but this type of formalism enabled us to link Gibbs free energy to the realistic CALPHAD thermodynamic database. The thermodynamics parameters used in this study are presented in Table.2.

Table 2: Thermodynamic parameters for the Fe-Mn-V-C quaternary system. Parameters were taken from Refs.[33, 34, 35, 36]

BCC
$G_{Fe}^{BCC} = -22451.451 + 887.16955T - 118.9TlnT - 14.169 \times 10^{-4}T^2$
$+7686800T^{-1} - 7.929 \times 10^{8}T^{-2} + 3.6 \times 10^{10}T^{-3} + 2.29603 \times 10^{31}T^{-9}$
$G_{Mn}^{BCC} = -70840 + 854.4548T + 24.9TlnT - 14.169 \times 10^{-4}T^2$
$+7686800T^{-1} - 7.929 \times 10^{8}T^{-2} + 3.6 \times 10^{10}T^{-3} + 1.656847 \times 10^{30}T^{-9}$
$G_{V}^{BCC} = 100516 + 645.5360T + 48.77TlnT - 45.149 \times 10^{-4}T^2$
$+1.2175 \times 10^{-7}T^3 + 7757260T^{-1} - 7.929 \times 10^{8}T^{-2} + 3.6 \times 10^{10}T^{-3} + 1.656847 \times 10^{30}T^{-9}$
$G_{C}^{BCC} = -17369 + 170.73T - 24.3TlnT - 4.723 \times 10^{-4}T^2$
$+2562600T^{-1} - 2.643 \times 10^{8}T^{-2} + 1.2 \times 10^{10}T^{-3}$
${}^{0}L_{Fe,Mn:C}^{BCC} = 34052 - 23.467T$
${}^{0}L_{Fe,V:C}^{BCC} = -23674 + 0.465T$
${}^{1}L_{Fe,V:C}^{BCC} = 8283$
${}^{0}L_{Fe:C}^{BCC} = -190T$
${}^{0}L_{Fe,V:C}^{BCC} = -10000$
${}^{0}L_{V:C}^{BCC} = -297868$

FCC
$G_{Fe}^{FCC} = 32800 + 457.10556T - 24.3TlnT - 4.723 \times 10^{-4}T^2$
$+2562600T^{-1} - 2.643 \times 10^{8}T^{-2} + 1.2 \times 10^{10}T^{-3}$
$G_{Mn}^{FCC} = -45600.41 + 498.2558T - 24.3TlnT - 4.723 \times 10^{-4}T^2$
$+2562600T^{-1} - 2.643 \times 10^{8}T^{-2} + 1.2 \times 10^{10}T^{-3}$
$G_{V}^{FCC} = -117302 + 262.57T - 41.750TlnT - 55.7101 \times 10^{-4}T^2$
$+590546T^{-1}$
${}^{0}L_{Fe,Mn:C}^{FCC} = 34052 - 23.467T$
${}^{1}L_{Fe,V:C}^{FCC} = -7645.5 - 2.069T$
${}^{0}L_{Fe:C}^{FCC} = -34671$
${}^{0}L_{Fe,V:C}^{FCC} = -10000$
${}^{1}L_{Mn:C}^{FCC} = -43433$ ${}^{0}L_{V:C}^{FCC} = -30394$

Cubic (NaCl)
$G_{Fe}^{Cubic_{NaCl}} = -27098.266 + 300.25256T - 46TlnT + 2.78854 \times 10^{31}T^{-9}$
$G_{Mn}^{Cubic_{NaCl}} = -3439.3 + 131.884T - 24.5177TlnT - 0.006t^2 + 69600T^{-1}$
$G_{V}^{Cubic_{NaCl}} = -430.43 + 135.046053T - 24.134TlnT - 0.003098T^2 + 1.2175 \times 10^{-7}T^3 + 69460T^{-1}$
${}^{0}L_{Fe,V:C}^{Cubic_{NaCl}} = -40000$
${}^{0}L_{Fe,Mn:C}^{Cubic_{NaCl}} = -7762 + 3.865T$
${}^{0}L_{Fe,Mn}^{Cubic_{NaCl}} = -7762 + 3.865T$
${}^{1}L_{Fe,Mn}^{Cubic_{NaCl}} = -259$
${}^{1}L_{Mn,V}^{Cubic_{NaCl}} = -11820$
${}^{1}L_{Fe,V}^{Cubic_{NaCl}} = -15291 - 4.138T$

The molar Gibbs energy of the whole system can be described as the sum of mo-

lar Gibbs energy of austenite and ferrite ($G^{\gamma,\alpha}$) and that of vanadium carbide MC precipitates which have a Cubic-NaCl crystal structure [5] ($G^{cubic_{NaCl}}$).

$$
\begin{aligned}
G(c_i, y^{(s)_i}) &= G^{\gamma,\alpha}(c_i) + \Delta G^{NaCl} \\
&= [\sum_i c_i G_i^{\gamma,\alpha} + RT \sum_i c_i ln c_i + \\
&\sum_i \sum_{j>i} c_i c_j \sum_{n=0}^{m} ({}^n L_{i:j}^{\gamma,\alpha} (c_i - c_j)^n) + \\
&\sum_i \sum_{j>i} \sum_{k>j} c_i c_j c_k L_{i,j:k}^{\gamma,\alpha}] + \sum_i \sum_j \sum_k y_i^{(1)} y_j^{(2)} y_k^{(3)} \Delta G_{i:j:k}^{NaCl} + \\
&\frac{RT}{4} \sum_s \sum_i y_i^{(s)} ln(y_i^{(s)}) \\
&+ \sum_s \sum_i \sum_{j>i} y_i^{(s)} y_j^{(s)} \sum_{n=0}^{1} ({}^n L_{i:j}^{NaCl} (y_i^{(s)} - y_j^{(s)}) \quad (2)
\end{aligned}
$$

where ${}^n L_{i,j}$ and ${}^n L_{i,j,k}$ are binary and ternary interaction parameters, respectively. The order parameters described in Eq.1 are substituted into Eq.2 to obtain the molar free Gibbs free energy for the α, γ and interphase precipitates, $cubic_{NaCl}$:

$$
\begin{aligned}
G^{\gamma/\alpha + cubic_{NaCl}} &= \sum_i c_i G_i^{\gamma/\alpha} + \sum_i \sum_{j>i} c_i c_j \sum_{n=0}^{m} {}^n L_{i,j}^{\gamma/\alpha} (c_i - c_j)^n \\
&+ \sum_i \sum_{j>i} \sum_{k>j} c_i c_j c_k L_{i,j,k}^{\gamma/\alpha} + 4 \sum_{i=Mn,C,V} U_{Fe,i} c_i^2 \sum_j \phi_i^{i^2} \\
&- 4 \sum_{i=Mn,C,V} \sum_{j>i} c_i c_j (U_{i,j} - U_{Fe,i} - U_{Fe,j}) \sum_k \phi_i^k \phi_j^k \\
&+ \frac{RT}{4} \left\{ \ A \ \right\} \\
&- 4 \left\{ \ B \ \right\}
\end{aligned}
$$

$$+ 4\alpha_{Mn,Fe,C} c_{Mn} c_C \left\{ \ C \ \right\} \quad (3)$$

$$\left\{ \ A \ \right\} =$$

$$\left\{ \begin{array}{c} \sum_{i=Mn,C,V,Mo}[c_i(1-\phi_i^1-\phi_i^2+\phi_i^3)]ln[c_i(1-\phi_i^1-\phi_i^2+\phi_i^3)] \\ +[1-\sum_{i=Mn,C,V,Mo} c_i(1-\phi_i^1-\phi_i^2+\phi_i^3)]ln[c_i(1-\phi_i^1-\phi_i^2+\phi_i^3)] \\ +\sum_{i=Mn,C,V,Mo}[c_i(1-\phi_i^1+\phi_i^2-\phi_i^3)]ln[c_i(1-\phi_i^1+\phi_i^2-\phi_i^3)] \\ +[1-\sum_{i=Mn,C,V,Mo} c_i(1-\phi_i^1+\phi_i^2-\phi_i^3)]ln[c_i(1-\phi_i^1+\phi_i^2-\phi_i^3)] \\ +\sum_{i=Mn,C,V,Mo}[c_i(1+\phi_i^1-\phi_i^2-\phi_i^3)]ln[c_i(1+\phi_i^1-\phi_i^2-\phi_i^3)] \\ +[1-\sum_{i=Mn,C,V,Mo} c_i(1+\phi_i^1-\phi_i^2-\phi_i^3)]ln[c_i(1+\phi_i^1-\phi_i^2-\phi_i^3)] \\ +\sum_{i=Mn,C,V,Mo}[c_i(1+\phi_i^1+\phi_i^2+\phi_i^3)]ln[c_i(1+\phi_i^1+\phi_i^2+\phi_i^3)] \\ +[1-\sum_{i=Mn,C,V,Mo} c_i(1+\phi_i^1+\phi_i^2+\phi_i^3)]ln[c_i(1+\phi_i^1+\phi_i^2+\phi_i^3)] \end{array} \right\} \quad (4)$$

$$\left\{ \ B \ \right\} =$$

$$\left\{ \begin{array}{c} 3^1L_{Mn,Fe}^{cubic_{NaCl}} c_{Mn}^2((2c_{Mn}-1)\sum_i \phi_{Mn}^{i^2} + 4c_{Mn}\phi_{Mn}^1\phi_{Mn}^2\phi_{Mn}^3) \\ -3^1L_{Fe,C}^{cubic_{NaCl}} c_C^2((2c_C-1)\sum_i \phi_C^{i^2} + 4c_C\phi_C^1\phi_C^2\phi_C^3) \\ -3^1L_{F,V}^{cubic_{NaCl}} c_V^2((2c_V-1)\sum_i \phi_V^{i^2} + 4c_V\phi_V^1\phi_V^2\phi_V^3) \\ -2\sum_i\sum_{j>i} c_i c_j({}^1L_{Fe,i}^{cubic_{NaCl}} - {}^1L_{Fe,j}^{cubic_{NaCl}})\sum_k \phi_i^k\phi_j^k \\ +2c_{Mn}c_Cc_V({}^1L_{Mn,Fe}^{cubic_{NaCl}} - {}^1L_{Fe,C}^{cubic_{NaCl}} - {}^1L_{Fe,V}^{cubic_{NaCl}})(\sum_{i=Mn,C,V}\sum_{j\neq i}\sum_{k\neq j\neq i}\phi_i^1\phi_j^2\phi_k^3 \\ +\sum_{i=Mn,C,V}\sum_{j>i}\sum_k \phi_i^k\phi_j^k) \\ -c_{Mn}^2c_V({}^1L_{Mn,V}^{cubic_{NaCl}} + {}^1L_{Fe,V}^{cubic_{NaCl}} - 3^1L_{Mn,Fe}^{cubic_{NaCl}})[2\sum_i\sum_{j\neq i}\sum_{k>j,k\neq i}\phi_V^i\phi_{Mn}^j\phi_{Mn}^k \\ +\sum_i(\phi_{Mn}^{i^2} + 2\phi_{Mn}^i\phi_V^i)] \\ -c_{Mn}^2c_C({}^1L_{Mn,C}^{cubic_{NaCl}} + {}^1L_{Fe,C}^{cubic_{NaCl}} - 3^1L_{Mn,Fe}^{cubic_{NaCl}})[2\sum_i\sum_{j\neq i}\sum_{k>j,k\neq i}\phi_C^i\phi_{Mn}^j\phi_{Mn}^k \\ +\sum_i(\phi_{Mn}^{i^2} + 2\phi_{Mn}^i\phi_C^i)] \\ +c_{Mn}c_V^2({}^1L_{Mn,V}^{cubic_{NaCl}} + {}^1L_{Mn,Fe}^{cubic_{NaCl}} - 3^1L_{Fe,C}^{cubic_{NaCl}})[2\sum_i\sum_{j\neq i}\sum_{k>j,k\neq i}\phi_{Mn}^i\phi_V^j\phi_V^k \\ +\sum_i(\phi_V^{i^2} + 2\phi_{Mn}^i\phi_V^i)] \\ -c_V^2c_C({}^1L_{V,C}^{cubic_{NaCl}} + {}^1L_{Fe,C}^{cubic_{NaCl}} - 3^1L_{Fe,V}^{cubic_{NaCl}})[2\sum_i\sum_{j\neq i}\sum_{k>j,k\neq i}\phi_C^i\phi_V^j\phi_V^k \\ +\sum_i(\phi_V^{i^2} + 2\phi_V^i\phi_C^i)] \\ +c_{Mn}c_C^2({}^1L_{Mn,C}^{cubic_{NaCl}} + {}^1L_{Mn,Fe}^{cubic_{NaCl}} - 3^1L_{Fe,C}^{cubic_{NaCl}})[2\sum_i\sum_{j\neq i}\sum_{k>j,k\neq i}\phi_{Mn}^i\phi_C^j\phi_C^k \\ +\sum_i(\phi_C^{i^2} + 2\phi_{Mn}^i\phi_C^i)] \\ -c_Vc_C^2(-{}^1L_{V,C}^{cubic_{NaCl}} + {}^1L_{Fe,V}^{cubic_{NaCl}} + 3^1L_{Fe,C}^{cubic_{NaCl}})[2\sum_i\sum_{j\neq i}\sum_{k>j,k\neq i}\phi_V^i\phi_C^j\phi_C^k \\ +\sum_i(\phi_C^{i^2} + 2\phi_V^i\phi_C^i)] \end{array} \right\} \quad (5)$$

$$\left\{ C \right\} =$$

$$\left\{ \begin{array}{c} -c_V^2(\sum_i \phi_{Mn}^i \phi_C^j + 1)\sum_i \phi_V^{i^2} + 4c_V^2 \sum_i \phi_{Mn}^i \phi_C^i \phi_V^{i^2} - (c_V - 1)^2 \sum_i \phi_{Mn}^i \phi_C^i \\ -\sum_{i=Mn,C} \sum_{j \neq i} c_i(3c_i + 2c_j + 2(c_V - 1)) \sum_k \phi_i^{k^2} \\ -2c_{Mn}c_C(\sum_i \phi_{Mn}^{i^2})(\sum_i \phi_C^{i^2}) + 8c_{Mn}c_C \sum_i \phi_{Mn}^{i^2} \phi_C^{i^2} \\ +4\sum_{i=Mn,C} \sum_{j \neq i} c_{Mn}\{\phi_j^1(\phi_i^1 - \phi_i^2\phi_i^3) + \phi_j^2(\phi_i^2 - \phi_i^1\phi_i^3) + \phi_j^3(\phi_i^3 - \phi_i^1\phi_i^2)\} \\ +4\sum_{i=Mn,C} \sum_{j \neq i} c_i c_V \left\{ \begin{array}{c} 2(\phi_i^1 - \phi_i^2\phi_i^3)(\phi_j^2\phi_V^3 + \phi_j^3\phi_V^2 - \phi_j^1\phi_V^1) \\ +2(\phi_i^2 - \phi_i^1\phi_i^3)(\phi_j^1\phi_V^3 + \phi_j^3\phi_V^1 - \phi_j^2\phi_V^2) \\ +2(\phi_i^3 - \phi_i^1\phi_i^2)(\phi_j^1\phi_V^2 + \phi_j^2\phi_V^1 - \phi_j^3\phi_V^3) \\ +4\sum_k \phi_i^{k^2}\phi_j^k\phi_V^k - (\sum_k \phi_i^{k^2} + 1)(\sum_k \phi_j^k\phi_V^k) \end{array} \right\} \\ +3\sum_{i=Mn,C} \sum_{j \neq i} c_i^2\{-(\sum_k \phi_i^{k^2} + 1)\sum_k \phi_i^k\phi_j^k + 2\sum_k \phi_i^{k^3}\phi_j^k \\ +2(\phi_j^1\phi_i^2\phi_i^3 + \phi_i^1\phi_j^2\phi_i^3 + \phi_i^1\phi_i^2\phi_j^3)\} + 2\sum_i \sum_{j>i} \sum_{k \neq j, k \neq i}(\phi_{Mn}^i\phi_C^j + \phi_{Mn}^j\phi_C^i \\ -\phi_{Mn}^k - \phi_C^k)(-c^2V\phi_V^i\phi_V^j - c_V\phi^k\phi_V^k + c_V^2\phi_V^k) \\ -8c_{Mn}c_C\{\sum_i \sum_{j \neq i} \sum_{k>j, k \neq i}(\phi_{Mn}^i - \phi_{Mn}^j\phi_{Mn}^k)(\phi_C^i - \phi_C^j\phi_C^k)\} \\ +6(c_{Mn}^2\phi_{Mn}^1\phi_{Mn}^2\phi_{Mn}^3 + c_C^2\phi_C^1\phi_C^2\phi_C^3) \end{array} \right\} \tag{6}$$

The total stress-free chemical free energy of the system in the Fe-Mn-C-V system can be expressed as [37]:

$$F \equiv \int_V (\frac{1}{V_m} G^{\alpha,\gamma or\ Cubic_{NaCl}} + \frac{\alpha}{2} \sum_{i=Mn,C,V}^{3} (\nabla c_i)^2 + [\frac{\beta}{2} \sum_{i=Mn,C,V}^{3} (\nabla \phi_i^j)^2])dV \tag{7}$$

Where, V_m is the molar volume which is considered to be constant equal to $7.3 * 10^-6\ m^3/mole$. α and β are the gradient energy coefficients for the compositions and order parameters, respectively. The temporal evolution of the elemental concentrations and order parameters can be determined by evaluating the following non-linear Cahn-

Hilliard diffusion equations and time-dependant Ginzburg-Landau equations:

$$\frac{\partial c_i}{\partial t} = \sum_j \nabla.(\tilde{M}_{ij} \nabla \frac{\delta F}{\delta c_j}), \quad i = Mn, C, V, \quad j = Mn, C, V \tag{8}$$

$$\frac{\partial \phi_i^j}{\partial t} = -L \frac{\delta F}{\delta \phi_i^j}, \quad i = Mn, C, V, \quad j = 1, 2, 3 \tag{9}$$

where, $\tilde{M}_{ij}$ and L are the diffusion mobility and the structural relaxation, respectively. The diffusion mobility, $\tilde{M}_{ij}$, was related by the atomic mobilities of Mn, V, C and Fe using the following equation[38]:

$$\tilde{M}_{ij} = \sum_n (\delta_{in} - c_i)(\delta_{jn} - c_j) c_n M_n^{Fe} \tag{10}$$

where, δ_{in} and δ_{jn} represent the Kronecker delta. diffusivity of Mn, V, and C in α and γ were taken to be $M_{Mn}^{\alpha,Fe} = 7.03881e^{-18}$, $M_{Mn}^{\gamma,Fe} = 7.23763e^{-20}$, $M_C^{\alpha,Fe} = 6.14251e^{-11}$, $M_C^{\gamma,Fe} = 3.67803e^{-13}$, $M_V^{\alpha,Fe} = 1.0552e^{-17}$, $M_V^{\gamma,Fe} = 1.55038e^{-19}$, respectively. The parameter *L* was determined by $\tilde{M}_C = La_0^2/16$ [39], where a_0 is the lattice parameter of the matrix. The binding energy of Mn to the interphase boundary was assumed to be 9.9 kJ/mol [40]. $\alpha_{Mn,Fe,C}$ was assumed to be 31270 $\mathrm{Jm}^2/\mathrm{mol}$ [34]. The value of the gradient coefficient β was 3.8×10^{-16}J/m. This value was observed by atom probe analyses [31] for multicomponent systems and gives the interphase interfacial diffuse chemical profile equating to $\sim$ 3 nm. The values for both coefficients α and β was considered to be the same for all phases involved for the sake of simplicity and in order to develop on single free energy function to describe the evolution. At the nucleation stage, small cells with a side of 1 nm were seeded to NaCl-type interphase precipitates after uniform random value was generated for nucleation sites at the inter-phase. For multi-particle simulations, the number of nucleus in the field was determined according to experimental observations reported in Ref.[31, 34]. These calculations are currently being done in our research group and will be presented in our future papers. The grid size was set to 0.5 nm with a total number of grids equal to 300×300×300. A Semi-Implicit-Fourier-Spectral-Method [41] was employed for numerical analysis with a periodical boundary condition.

3. Experimental Validation and Discussion

A three dimensional simulation for the microstructural development of an Fe-Mn-V-C quaternary system isothermally transformed at 973 K was performed through directly linking free energy calculations to the CALPHAD method. The simulation for a single interphase precipitate growing on a stationary γ/α interphase boundary shows that the particle has a disk-like shape (Fig.2) similar to the abutted spherical caps predicted morphology for grain boundary precipites considered by Clemm and Fisher [42]. The predictions of which are shown in Figures 3, 4 and 5. The cross-sectional compositional evolution of the precipitates growing along the γ/α interphase boundary are also shown in each figure accompanying each image of the growing precipitate after a given number of modelled time steps. After the formation of nuclei, the particles were found to be supersaturated with C of 11.1 at%, as shown in Fig.3. The degree of supersaturation then continuously decreased as the precipitates grew, as is evident from Fig.4 until it reached the equilibrium value of 8 at%. The partitioning of Mn and V atoms into the precipitates, however, was not as rapid as that of C due to the smaller diffusivity of substitutional alloying elements compared to that of C atoms.

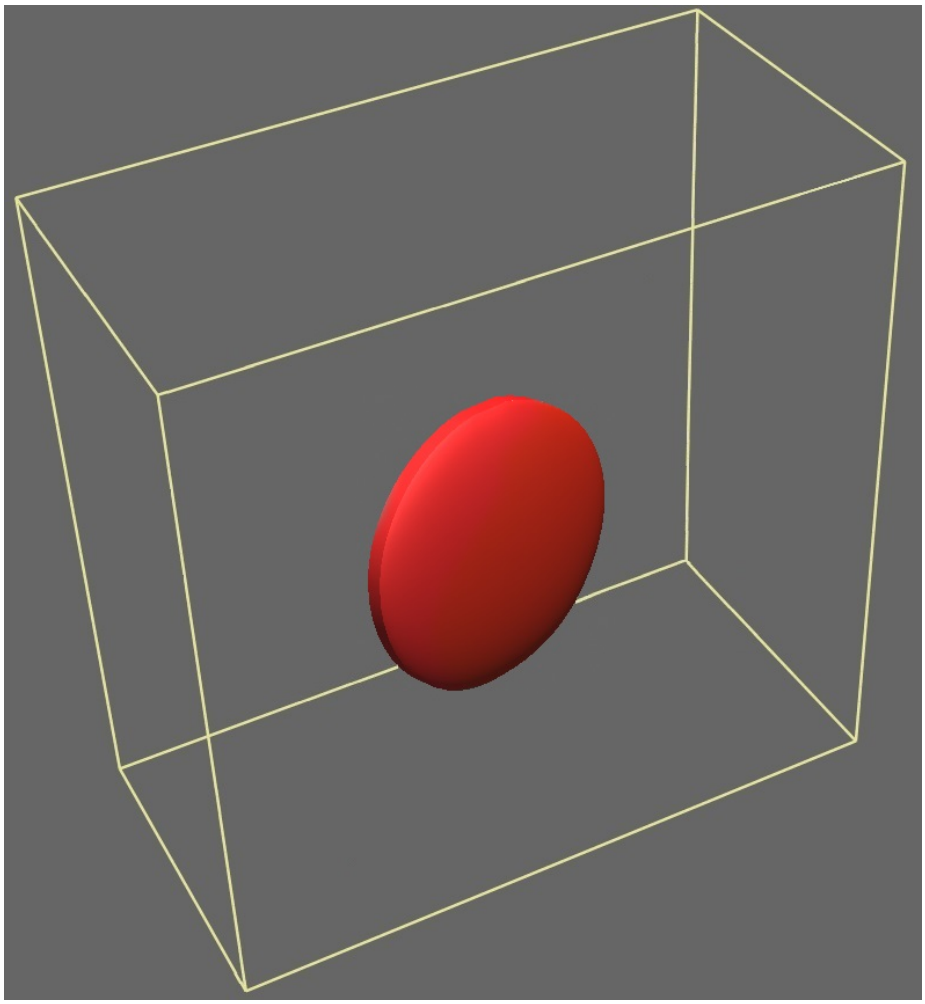

Figure 2: Oblate spheroid morphology of a single interphase precipitate after 6000 Δt steps.

The modelled interphase precipitate composition, and oblate spheroid morphology in Figure 4 is in strong accordance with the dual SAX and SANS scattering interpretations of Oba *et al.* [26]. At 973 K Oba *et al.* [26] measured an average diameter of the precipitates as 23 nm this is very similar to our model prediction after 2000 Δt steps. However, some discrepancy is found if the model predictions are compared with the recent 3D APT studies of Mukherjee *et al.* [31, 32] where, a precursor nano-cluster to the interphase precipitates are observed and are found to significantly enriched in Ti and Mo elements rather than C. This is thought to be due to the fact that Ti and Mo exhibit

a significant solute drag effect upon the γ/α interphase boundary and are significantly enriched locally at the interphase boundary. Mo and Ti were not considered in this study. In respect to V however, the binding energy with the γ/α interphase boundary is thought to be far less significant in comparison to that of Ti and Mo [43]. V segregation and consequentially supersaturation in the precipitates therefore, would not be expected to be large at a moving γ/α interphase boundary [44]. This was experimentally observed using 3D APT in a V micro-alloyed steel by Nöhrer *et al.* [8]. The model is found to predict predict the observed enrichment of Mn in the interphase precipitates which is not found would not be the case for general heterogeneous precipitation.

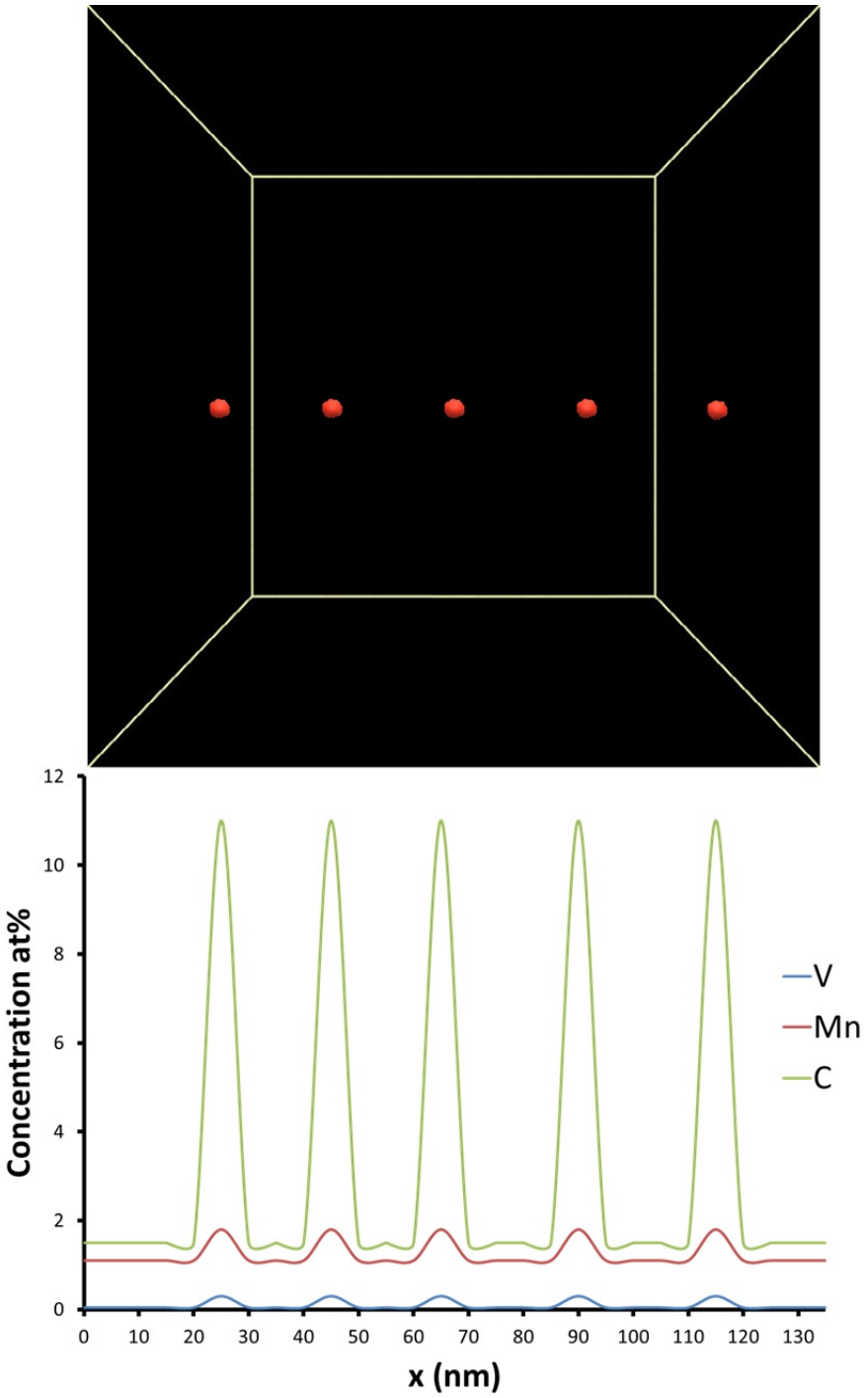

Figure 3: Morphology, size of growing interphase precipitates after 500 Δt steps and cross-sectional composition profile of Mn, V and C at the γ/α interphase boundary in respect to x.

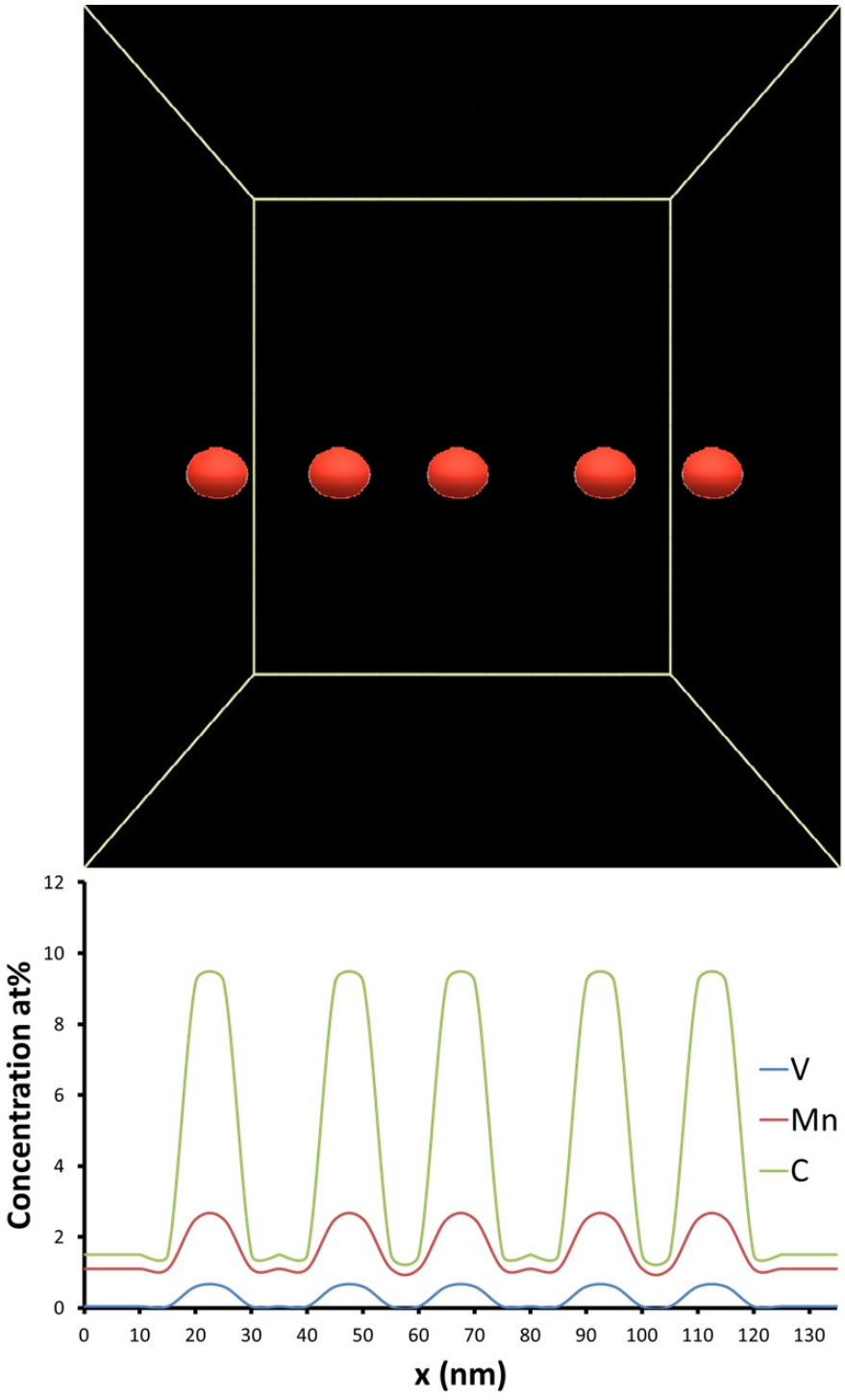

Figure 4: Morphology, size of growing interphase precipitates after 2000 Δt steps and cross-sectional composition profile of Mn, V and C at the γ/α interphase boundary in respect to x.

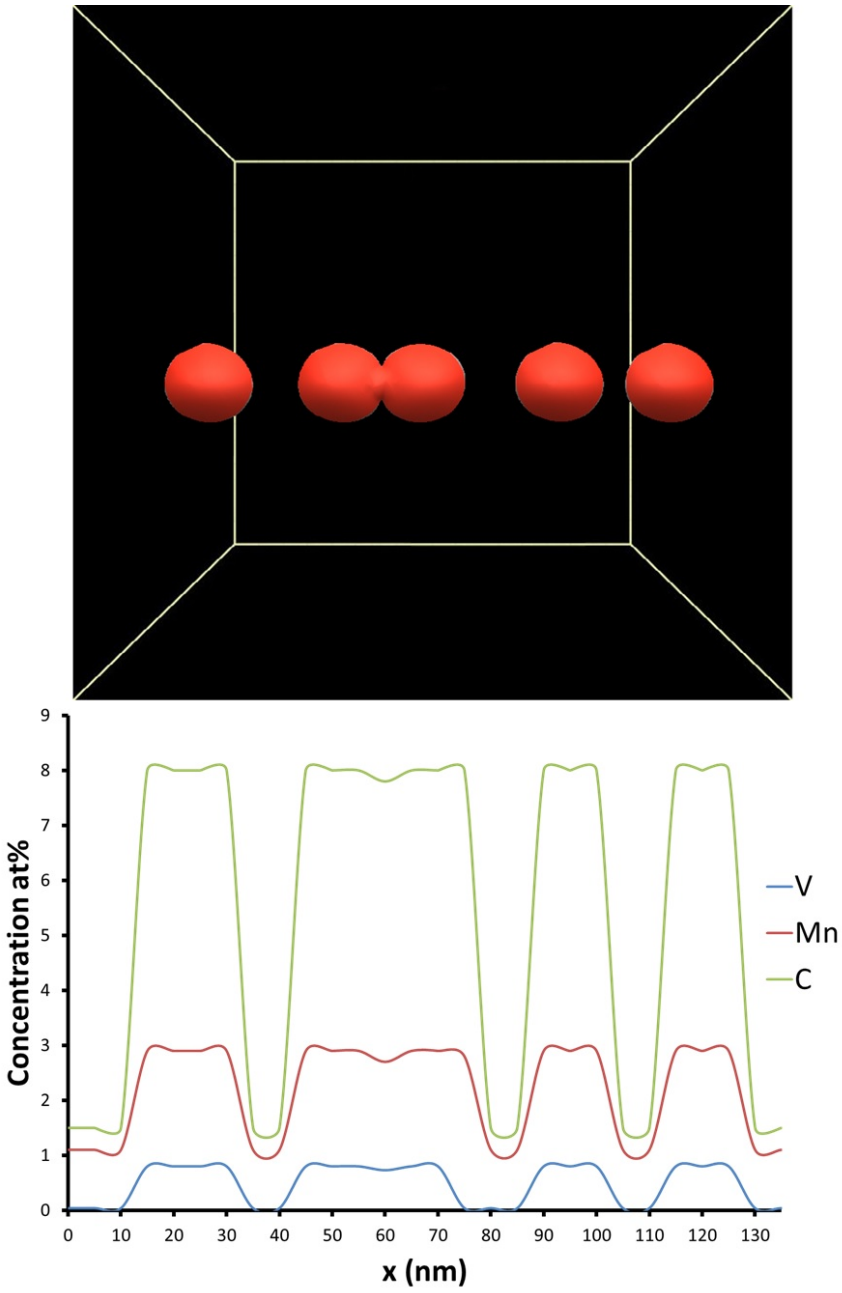

Figure 5: Morphology, size of growing interphase precipitates after 6000 Δt steps and cross-sectional composition profile of Mn, V and C at the γ/α interphase boundary in respect to x.

Although widely assumed, including implicitly in this work, the mobile γ/α in-

terphase interface does not always obey the KS OR. The studies by Law *et al.*[45], Okamoto *et al.*[10] and, Yen *et al.* [46] and recently the studies of Furuhara and co-workers[28, 29, 30] have elucidated the role of γ/α OR upon interphase precipitation and shown that interphase precipitation is not solely related to the KS interphase boundary. In particular, Zhang *et al.*[29, 30] have shown that interphase precipitate density increases with increasing misorientation from an ideal KS interphase boundary.

Recently, it has been observed that in some circumstances, in regions where planar interphase precipitation is exhibited the precipitates appear to exist in pairs, where the oblate spheroid precipitates appear to join at the tips [47]. The reason for this phenomena has yet to be resolved. However, it can be observed when in the 3D APT of Zhang *et al.*[29, 30], where precipitates pairing at the tips can be seen at relatively low transformation temperatures and relatively small values of γ/α $\Delta\theta$, although not equal to 0 missorietation from the ideal KS OR.

As shown in fig.5, two precipitates paired together at final stages of the simulation. The pairing occurred in order to decrease their interfacial energies. To elucidate the pairing between these two particular precipitates, the order parameter of Mn after $6000\Delta t$ steps is presented in Fig.6. These two precipitates of interest are indicated by numbers 2 and 3. As shown in this figure, the domain of precipitate 2 was the same as that of 3 while those of other precipitates were different. This phenomenon is very similar to the precipitation behaviour in super-alloys and light weight steels, where precipitates pair together to reduce their anti-phase boundary (APB) energy [24].

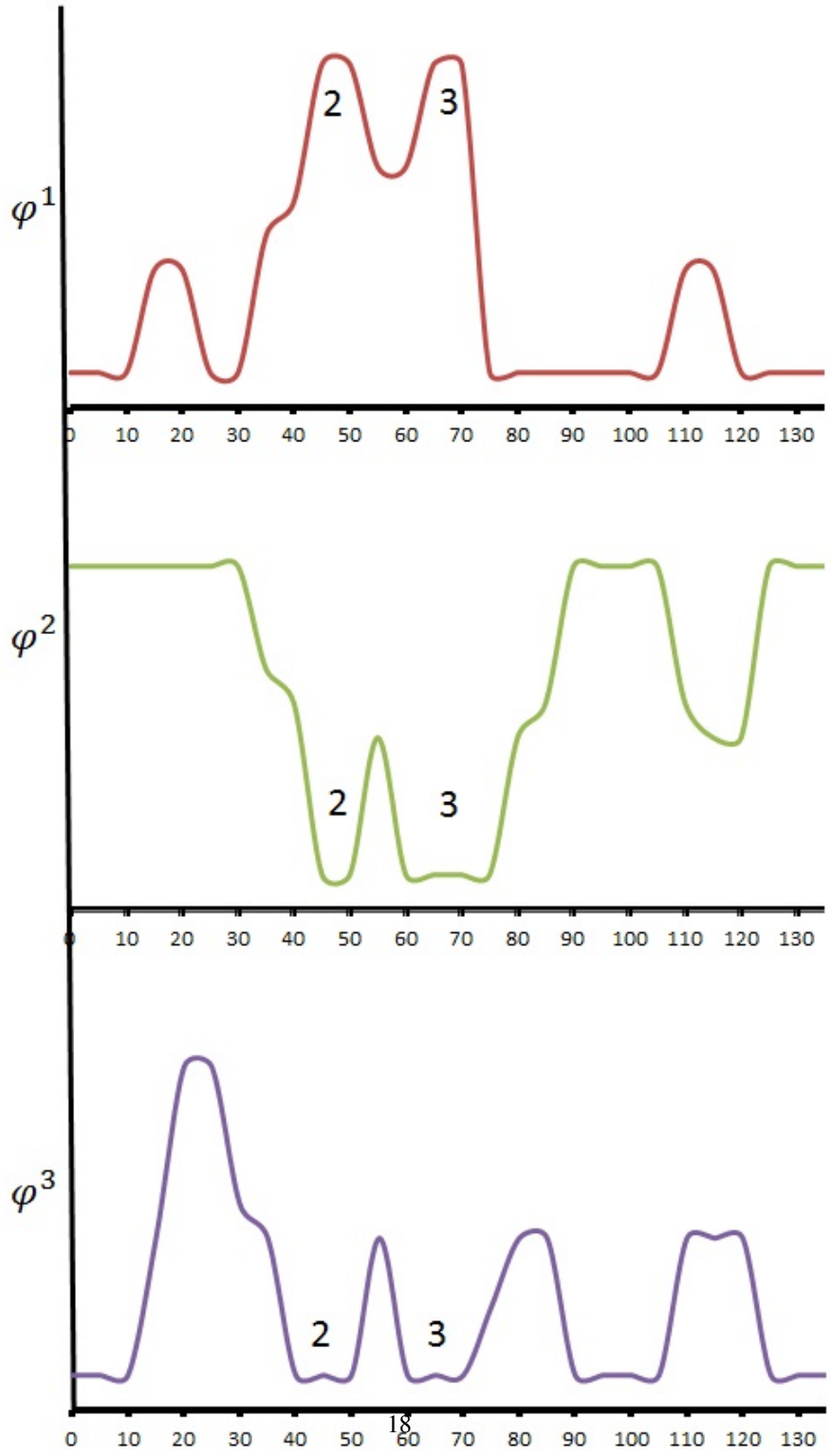

Figure 6: Order parameter profile of Mn in Fig.5.

4. Conclusions

A multi-component phase field model was developed for the simulation of interphase precipitation of carbide precipitates in steels. The model was directly coupled with thermodynamic data from the CALPHAD method using a four-sub-lattice model. Interphase carbide precipitation at the γ/α interface was simulated. The developed model has been used to elucidate the mechanisms for interphase precipitate growth with particular reference to vanadium carbide precipitation in medium-carbon micro-alloyed steels isothermally transformed at 973 K.

The model is found to be able to accurately predict:

1. *Interphase precipitate composition*, is in accordance with the dual SAX and SANS study of Oba *et al.* [26]. Our model does predict the observed enrichment of Mn.

2. *Morphology* the model is found to accurately predict oblate spheroid precipitates and their size.

3. The phenomena *tip-to-tip* pairing of interphase precipitates in γ/α interphase boundaries found to be attributable to the minimisation of interfacial energy.

5. Acknowledgement

Authors are thankful for financial support from the EPSRC grant EP/L018632/1 "Micro-structuring micro-alloyed steels via non-metallic precipitate formation" and financial assistance from the WMG Centre High Value Manufacturing Catapult are gratefully acknowledged.

References

[1] C. M. Sonsino, Light-weight design chances using high-strength steels, Materwiss. Werksttech. 38 (1) (2007) 9–22. doi:10.1002/mawe.200600090.

[2] R. A. Rijkenberg, A. Blowey, P. Bellina, C. Wooffindin, Advanced High Stretch-Flange Formability Steels for Chassis & Suspension Applications 3 . Product concept : tensile properties and microstructure (2014).

[3] Y. Funakawa, T. Shiozaki, K. Tomita, T. Yamamoto, E. Maeda, Development of High Strength Hot-rolled Sheet Steel Consisting of Ferrite and Nanometer-sized Carbides, ISIJ Int. 44 (11) (2004) 1945–1951. doi:10.2355/isijinternational.44.1945.

[4] R. W. K. Honeycombe, Transformation from austenite in alloy steels, Metall. Trans. A 7 (July) (1976) 915–936. doi:10.1007/BF02644057.

[5] R. Lagneborg, B. Hutchinson, T. Siwecki, S. Zajac, The Role of Vanadium in Microalloyed Steels, 2nd Edition, no. June, Swerea KIMAB, Stockholm, 2014.

[6] H.-W. Yen, C.-Y. Huang, J.-R. Yang, Characterization of interphase-precipitated nanometer-sized carbides in a Ti-Mo-bearing steel, Scr. Mater. 61 (6) (2009) 616–619. doi:10.1016/j.scriptamat.2009.05.036.
URL http://dx.doi.org/10.1016/j.scriptamat.2009.05.036

[7] A. T. Davenport, R. Honeycombe, Precipitation of carbides at y-a boundaries in alloy steels, Proc. R. Soc. London A 322 (1549) (1971) 191–205.

[8] M. Nöhrer, S. Zamberger, S. Primig, H. Leitner, Atom probe study of vanadium interphase precipitates and randomly distributed vanadium precipitates in ferrite, Micron 54-55 (2013) 57–64. doi:10.1016/j.micron.2013.08.008.
URL http://dx.doi.org/10.1016/j.micron.2013.08.008

[9] R. M. Smith, D. P. Dunne, Structural aspects of alloy carbonitride precipitation in microalloyed steels, Mater. Forum 11 (1988) 166–181.

[10] R. Okamoto, A. Borgenstam, J. Ågren, Interphase precipitation in niobium-microalloyed steels, Acta Mater. 58 (14) (2010) 4783–4790. doi:10.1016/j.actamat.2010.05.014.
URL http://linkinghub.elsevier.com/retrieve/pii/S1359645410002892

[11] J. K. Lee, H. I. Aaronson, Influence of faceting upon the equilibrium shape of nuclei at grain boundaries-II. Three-dimensions, Acta Metall. 23 (7) (1975) 809–820.

[12] H. K. D. H. Bhadeshia, Diffusional Transformations: A theory for the formation of superledges, Phys. Status Solidi a-Applied Res. 69 (2) (1982) 745–750.

[13] J. A. Todd, P. Li, S. M. Copley, A new model for precipitation at moving interphase boundaries, Metall. Trans. A 19 (September) (1988) 2133–2138. doi:10.1007/BF02645038.

[14] W. J. Liu, Computer simulation of VC Precipitation at Moving γ/α Interfaces, Metall. Trans. A 24 (10) (1993) 2195–2207. doi:10.1007/BF02648594.
URL http://www.springerlink.com/index/10.1007/BF02648594

[15] P. R. Rios, Morphology of interphase precipitation in microalloyed steels, J. Mater. Sci. Lett. 10 (1991) 981–983. doi:10.1007/BF00722153.

[16] P. R. Rios, A model for interphase precipitation in stoichiometrically balanced vanadium steels, J. Mater. Sci. 30 (1995) 1872–1878. doi:10.1007/BF00351624.

[17] R. Lagneborg, S. Zajac, A model for interphase precipitation in V-microalloyed structural steels, Metall. Mater. Trans. A 31 (001) (2001) 1–12.
URL http://link.springer.com/article/10.1007/s11661-001-0249-9

[18] M.-Y. Chen, M. Gouné, M. Militzer, Y. Bréchet, J.-R. Yang, Superledge Model for Interphase Precipitation During Austenite-to-Ferrite Transformation, Metall. Mater. Trans. A 45 (12) (2014) 5351–5361. doi:10.1007/s11661-014-2486-8.
URL http://link.springer.com/10.1007/s11661-014-2486-8

[19] M.-Y. Chen, M. Gouné, M. Verdier, Y. Bréchet, J.-R. Yang, Interphase precipitation in vanadium-alloyed steels: Strengthening contribution and morphological variability with austenite to ferrite transformation, Acta Mater. 64 (2014) 78–92. doi:10.1016/j.actamat.2013.11.025.
URL http://linkinghub.elsevier.com/retrieve/pii/S1359645413008756

[20] S. Clark, V. Janik, Y. Lan, S. Sridhar, Interphase Precipitation An Interfacial Segregation Model, ISIJ Int. 57 (3).

[21] H. I. Aaronson, M. R. Plichta, G. W. Franti, K. C. Russell, Precipitation at interphase boundaries, Metall. Trans. A 9 (3) (1978) 363–371. doi:10.1007/BF02646386.

[22] L.-Q. Chen, Phase -Field Models for Microstructure Evolution, Annu. Rev. Mater. Res. 32 (1) (2002) 113–140. doi:10.1146/annurev.matsci.32.112001.132041.
URL http://www.annualreviews.org/doi/abs/10.1146/annurev.matsci.32.112001.132041

[23] M. Militzer, Phase field modeling of microstructure evolution in steels, Curr. Opin. Solid State Mater. Sci. 15 (3) (2011) 106–115. doi:10.1016/j.cossms.2010.10.001.
URL http://dx.doi.org/10.1016/j.cossms.2010.10.001

[24] A. Rahnama, R. Dashwood, S. Sridhar, A phase-field method coupled with CALPHAD for the simulation of ordered ordered k-cabide precipitates in both disorered gamman and alpha phases in low density steel, Comput. Mater. Sci. 126 (2017) 152–159. doi:10.1016/j.commatsci.2016.09.015.
URL http://linkinghub.elsevier.com/retrieve/pii/S0927025616304566

[25] G. Miyamoto, R. Hori, B. Poorganji, T. Furuhara, Interphase precipitation of VC and resultant hardening in V-added medium carbon steels, ISIJ Int. 51 (10)

(2011) 1733–1739. doi:10.2355/isijinternational.51.1733.
URL http://www.scopus.com/inward/record.url?eid=2-s2.0-82455184379{&}partnerID=40{&}md5=58d1e60f8a2651d957d6c5fac7b56dbe

[26] Y. Oba, S. Koppoju, M. Ohnuma, T. Murakami, H. Hatano, K. Sasakawa, A. Kitahara, J. Suzuki, Quantitative Analysis of Precipitate in Vanadium-microalloyed Medium Carbon Steels Using Small-angle X-ray and Neutron Scattering Methods, ISIJ Int. 51 (11) (2011) 1852–1858. doi:10.2355/isijinternational.51.1852.

[27] T. Murakami, H. Hatano, G. Miyamoto, T. Furuhara, Effects of Ferrite Growth Rate on Interphase Boundary Precipitation in V Microalloyed Steels, ISIJ Int. 52 (4) (2012) 616–625. doi:10.2355/isijinternational.52.616.
URL http://joi.jlc.jst.go.jp/JST.JSTAGE/isijinternational/52.616?from=CrossRef

[28] G. Miyamoto, R. Hori, B. Poorganji, T. Furuhara, Crystallographic Analysis of Proeutectoid Ferrite/Austenite Interface and Interphase Precipitation of Vanadium Carbide in Medium-Carbon Steel, Metall. Mater. Trans. A 44 (8) (2013) 3436–3443. doi:10.1007/s11661-013-1702-2.
URL http://link.springer.com/10.1007/s11661-013-1702-2

[29] Y.-J. Zhang, G. Miyamoto, K. Shinbo, T. Furuhara, Effects of α/γ orientation relationship on VC interphase precipitation in low-carbon steels, Scr. Mater. 69 (1) (2013) 17–20. doi:10.1016/j.scriptamat.2013.03.020.
URL http://linkinghub.elsevier.com/retrieve/pii/S1359646213001814

[30] Y. Zhang, G. Miyamoto, K. Shinbo, T. Furuhara, T. Ohmura, T. Suzuki, K. Tsuzaki, Effects of transformation temperature on VC interphase precipitation and resultant hardness in low-carbon steels, Acta Mater. 84 (2015) 375–384.

doi:10.1016/j.actamat.2014.10.049.
URL http://dx.doi.org/10.1016/j.actamat.2014.10.049

[31] S. Mukherjee, I. B. Timokhina, C. Zhu, S. P. Ringer, P. D. Hodgson, Three-dimensional atom probe microscopy study of interphase precipitation and nanoclusters in thermomechanically treated titanium-molybdenum steels, Acta Mater. 61 (7) (2013) 2521–2530. doi:10.1016/j.actamat.2013.01.028.
URL http://dx.doi.org/10.1016/j.actamat.2013.01.028

[32] S. Mukherjee, I. B. Timokhina, C. Zhu, S. P. Ringer, P. D. Hodgson, Clustering and precipitation processes in a ferritic titanium-molybdenum microalloyed steel, J. Alloys Compd. 690 (2017) 621–632. doi:10.1016/j.jallcom.2016.08.146.
URL http://dx.doi.org/10.1016/j.jallcom.2016.08.146

[33] P. Gustafson, Thermodynamic evaluation of the Fe-C System, Scand. J. Metall. 14 (5) (1985) 259–267.

[34] W. Huang, Thermodynamic properties of the Fe-Mn-VC system, Metall. Trans. A 22 (September) (1991) 1911–1920.
URL http://link.springer.com/article/10.1007/BF02669859

[35] K. Frisk, Thermodynamic modelling of multicomponent cubic Nb, Ti and V carbides/carbonitrides, Calphad Comput. Coupling Phase Diagrams Thermochem. 32 (2) (2008) 326–337. doi:10.1016/j.calphad.2007.11.007.

[36] V. Raghavan, C-Fe-N-Nb-V (Carbon-Iron-Nitrogen-Niobium-Vanadium), J. Phase Equilibria Diffus. 33 (5) (2012) 1–3. doi:10.1007/s11669-012-0105-1.

[37] J. W. Cahn, J. Hilliard, Free Energy of a Nonuniform System. I. Interfacial Free Energy, J. Chem. Phys. 28 (2) (1958) 258–267. arXiv:9809069v1, doi:

10.1063/1.1744102.
URL http://dx.doi.org/10.1063/1.1744102

[38] T. Kitashima, T. Yokokawa, A. C. Yeh, H. Harada, Analysis of element-content effects on equilibrium segregation at gamma/gamma-prime interface in Ni-base superalloys using the cluster variation method, Intermetallics 16 (6) (2008) 779–784. doi:10.1016/j.intermet.2008.02.015.

[39] R. Poduri, L.-Q. Chen, Computer simulation of atomic ordering and compositional clustering in the pseudobinary Ni3AlNi3V system, Acta Mater. 46 (5) (1998) 1719–1729. doi:10.1016/S1359-6454(97)00335-2.

[40] H. Chen, S. van der Zwaag, A general mixed-mode model for the austenite-to-ferrite transformation kinetics in FeCM alloys, Acta Mater. 72 (2014) 1–12. doi:10.1016/j.actamat.2014.03.034.
URL http://www.sciencedirect.com/science/article/pii/S1359645414001815

[41] L.-Q. Chen, J. Shen, Applications of semi-implicit Fourier-spectral method to phase field equations, Comput. Phys. Commun. 108 (2-3) (1998) 147–158. doi:10.1016/S0010-4655(97)00115-X.
URL http://www.sciencedirect.com/science/article/pii/S001046559700115X

[42] P. Clemm, J. Fisher, The influence of grain boundaries on the nucleation of secondary phases, Acta Metall. 3 (1955) 70–73.

[43] H. Jin, I. Elfimov, M. Militzer, Study of the interaction of solutes with $\Sigma 5$ (013) tilt grain boundaries in iron using density-functional theory, J. Appl. Phys. 115 (9). doi:10.1063/1.4867400.

[44] G. R. Purdy, Y. J. M. Bréchet, A solute drag treatment of the effects of alloying elements on the rate of the proeutectoid ferrite transformation in steels, Acta Metall. Mater. 43 (10) (1995) 3763–3774. doi:10.1016/0956-7151(95)90160-4.

[45] N. C. Law, S. A. Parsons, P. R. Howell, D. V. Edmonds, Crystallography of carbide precipitation at transformation interfaces during austenite decomposition in a low-alloy steel, Mater. Sci. Technol. 3 (8) (1987) 642–648. doi:10.1179/026708387790329559.

[46] H.-W. Yen, P.-Y. Chen, C.-Y. Huang, J.-R. Yang, Interphase precipitation of nanometer-sized carbides in a titaniummolybdenum-bearing low-carbon steel, Acta Mater. 59 (16) (2011) 6264–6274. doi:10.1016/j.actamat.2011.06.037.
URL http://linkinghub.elsevier.com/retrieve/pii/S1359645411004514

[47] A. Chamisa, Development of Ultra High Strength Steels for Reduced Carbon Emissions in Automotive Vehicles, Ph.D. thesis, University of Sheffield (2014).
URL http://etheses.whiterose.ac.uk/6274/